HVAC&R Research

ISSN: 1078-9669 (Print) 1938-5587 (Online) Journal homepage: http://www.tandfonline.com/loi/uhvc20

Virtual Refrigerant Pressure Sensors for Use in Monitoring and Fault Diagnosis of Vapor-Compression Equipment

Haorong Li & James E. Braun

To cite this article: Haorong Li & James E. Braun (2009) Virtual Refrigerant Pressure Sensors for Use in Monitoring and Fault Diagnosis of Vapor-Compression Equipment, HVAC&R Research, 15:3, 597-616

To link to this article: https://doi.org/10.1080/10789669.2009.10390853

Virtual Refrigerant Pressure Sensors for Use in Monitoring and Fault Diagnosis of Vapor-Compression Equipment

Haorong Li, PhD
Member ASHRAE

James E. Braun, PhD, PE
Fellow ASHRAE

Received July 7, 2008; accepted October 2, 2008

Refrigerant pressures are critical measurements for monitoring, control, diagnostics, and optimization of vapor compression cycle equipment. Direct refrigerant pressure measuring practices are expensive and more than often problematic. This paper describes a method, termed virtual pressure sensing*, wherein refrigerant pressure values are indirectly derived from low-cost temperature sensors that can be surface-mounted. In this manner, physical pressure sensors are eliminated and pressure sensing can be achieved at a much lower cost and in a non-invasive way. Five virtual pressure sensors are developed to obtain the five most important pressures in vapor compression cycle equipment: compressor discharge line pressure, condensing pressure, liquid line pressure, evaporating pressure, and suction line pressure. The performance of the proposed virtual pressure sensors, in terms of accuracy in estimating pressures and inferring liquid line subcooling, suction superheat, compressor power consumption, and refrigerant flow rate, is evaluated extensively using laboratory data collected from four systems. These systems include air conditioners and heat pumps, split and packaged systems, refrigerants R-22 and R-410a, fixed-orifices and thermal expansion valves, and reciprocating compressors and scroll compressors. Ultimately, the virtual sensors are used as a part of a decoupling-based fault detection and diagnosis (FDD) technique to diagnose multiple simultaneous faults. The impact of the virtual pressure sensors on the FDD performance is evaluated extensively using the laboratory data collected from the four various systems.*

INTRODUCTION

Refrigerant pressures are critical measurements for performance monitoring, control, diagnostics, and optimization of vapor compression cycle equipment. They are typically used as inputs in determining evaporating and condensing temperatures, liquid line subcooling, and suction line superheat. These quantities are used for equipment monitoring and within diagnostic algorithms (Rossi and Braun 1997; Li and Braun 2003; Cui and Wang 2005; Reddy 2007; Li and Braun 2007a). They can also be used in combination with compressor maps to predict refrigerant mass flow and power consumption and thus system efficiency and capacity (Li and Braun 2007b; Reddy 2007) for performance monitoring and fault impact evaluation, and they can be used to derive decoupling features (Li and Braun 2007b; Li and Braun 2008) that provide an indication of fault levels.

Pressure measurements are relatively expensive, and their use has been an impediment to the development of cost-effective embedded diagnostic systems. Accurate pressure sensors are

Haorong Li is an assistant professor of Architecture Engineering at the University of Nebraska-Lincoln, Omaha, NE. **James E. Braun** is a professor in the Ray W. Herrick Laboratories, School of Mechanical Engineering, Purdue University, West Lafayette, IN.

much more expensive than temperature sensors (Li and Braun 2007c). Furthermore, the cost of installing pressure sensors in the field can be expensive. Ideally, connections for permanent installation of pressure sensors should be brazed to the suction and discharge piping for the compressor. For field installations, this requires that refrigerant be evacuated and recharged, which is an expensive procedure. If pressure sensors are permanently connected to available threaded service ports on the compressor, then it is likely that refrigerant will leak over time (Li and Braun 2006).

The objective of the work described in this paper is to remove physical pressure sensors and estimate the compressor discharge line pressure, condensing pressure, liquid line pressure, evaporating pressure, and suction line pressure using low-cost temperature sensors. The performance should be robust against variations in driving conditions and all kinds of faults.

To this end, the starting point is that evaporator and condenser pressures can be estimated using the knowledge that refrigerant is a two-phase mixture somewhere in both the condenser and evaporator as long as the system is not severely undercharged (i.e., 80% or less than its nominal charge). If the saturation temperature can be accurately and reliably measured, then saturation pressure can be estimated using refrigerant property correlations. The evaporating and condensing temperatures can be estimated by using thermocouples that are soldered to the surface of return bends at suitable locations and then insulated from the environment. However, there are several technical issues that need to be considered, including 1) identifying suitable locations for mounting thermocouples that will ensure that refrigerant conditions are saturated for a wide range of driving conditions and in the presence of all kinds of faults, 2) accounting for the pressure drop between locations where temperatures are measured and the points where virtual pressure measurements are needed, and 3) evaluating the overall accuracy and impact on diagnostic performance of employing virtual pressure measurements. The section in this paper titled "Development of Virtual Pressure Sensors" describes the technical development of virtual pressure sensors and addresses sensor locations and pressure drop estimations. The section titled "Laboratory Evaluations of Virtual Pressure Sensors" provides an extensive evaluation in terms of accuracy in estimating pressures and quantities derived from pressure and other measurements, including liquid line subcooling, suction superheat, compressor power consumption, and refrigerant flow rate. The evaluation uses laboratory data for a number of different systems tested over a large range of operating conditions. In the section titled "Diagnosing Multiple Simultaneous Faults Using Virtual Pressure Sensors," the virtual sensors are used as a part of a decoupling-based fault detection and diagnosis (FDD) technique (Li and Braun 2007a, 2007b, 2008) to diagnose multiple simultaneous faults and the impact of the virtual pressure sensors on the FDD performance is evaluated extensively.

DEVELOPMENT OF VIRTUAL PRESSURE SENSORS

Overview of General Approach

Figure 1 illustrates a typical vapor-compression system. The system includes four major components: compressor, condenser, expansion device, and evaporator. There is also piping between components, including a discharge line between the compressor and condenser, a liquid line connecting the condenser to the expansion device, and a suction line between the evaporator and compressor. The expansion device is usually located in close proximity to the evaporator with small feeder tubes that distribute refrigerant to individual evaporator flow circuits.

Two types of condenser structures are illustrated in Figures 2 and 3. The Type I structure uses two separate circuiting arrangements to handle the desuperheating, condensing, and subcooling of the refrigerant, whereas the Type II uses three circuiting arrangements. The Type I condenser in Figure 2 has $n_{cond,1}$ parallel desuperheating and condensing circuits with $m_{cond,1}$

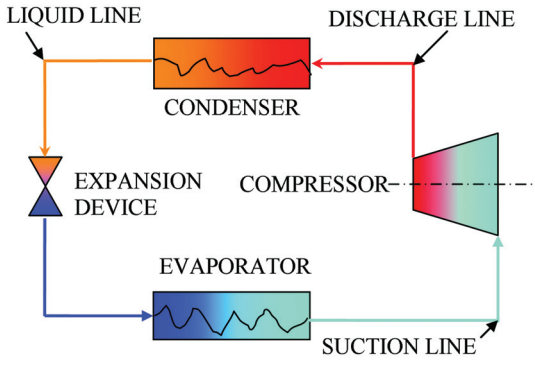

Figure 1. Block diagram for a typical vapor compression system.

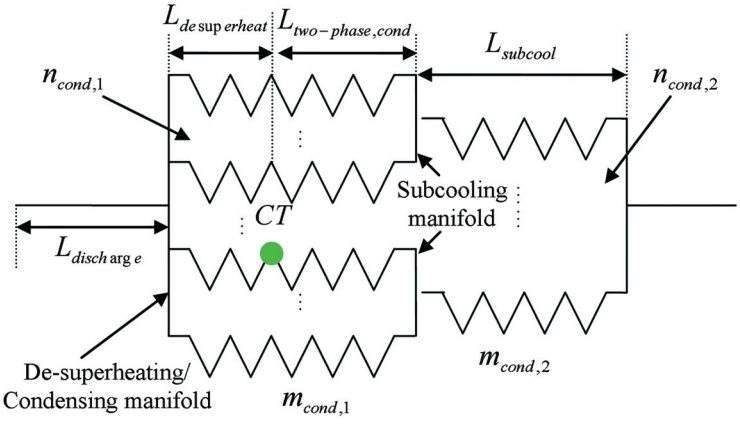

Figure 2. Type I condenser structure and sensor location.

passes within each circuit, then combines into $n_{cond,2}$ subcooling circuits with $m_{cond,2}$ passes within each circuit. This type of condenser is commonly used for residential and small commercial rooftop unit systems. The Type II condenser in Figure 3 has $n_{cond,1}$ parallel desuperheating circuits with $m_{cond,1}$ passes on each circuit, then combines into $n_{cond,2}$ condensing circuits with $m_{cond,2}$ passes on each circuit, and finally combines into $n_{cond,3}$ subcooling circuits with $m_{cond,3}$ passes on each circuit. Type II condenser arrangements are not very common in modern equipment.

Figure 4 shows a typical evaporator arrangement that utilizes n_{evap} parallel refrigerant circuits with m_{evap} passes within each circuit.

For both the evaporator and condenser, there is typically a portion of each heat exchanger (HX) that always contains a two-phase mixture of refrigerant under steady-state conditions. Therefore, if a suitable location can be identified and the temperature can be reliably measured, then saturation pressures can be inferred from temperature measurements. However, it is necessary to identify appropriate locations within the condenser and evaporator for measuring saturation temperatures and to estimate pressure drops between these locations and other locations where the pressure measurements are needed. Figure 5 illustrates the virtual pressure sensor development concept. The first step is to identify and demonstrate robust locations

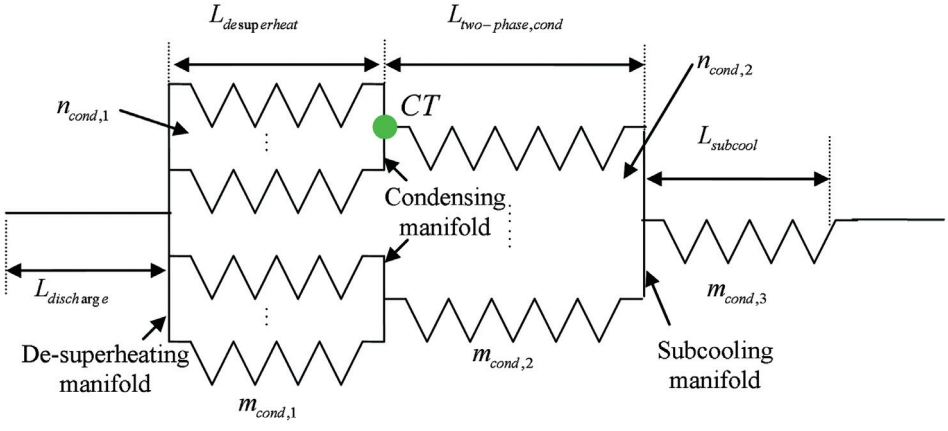

Figure 3. Type II condenser structure and sensor location.

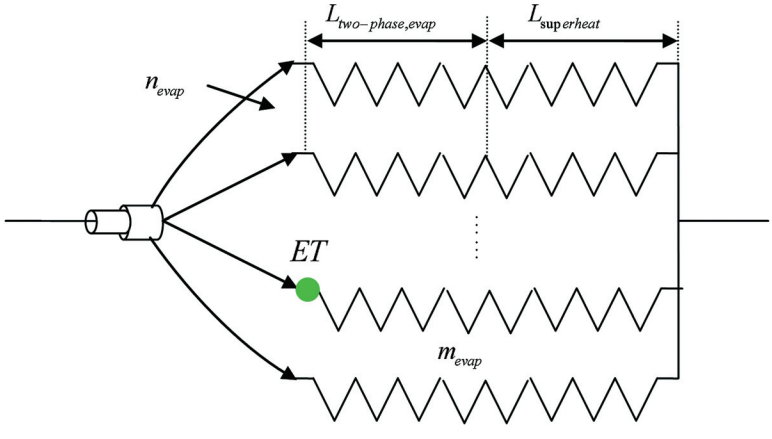

Figure 4. A typical evaporator structure and sensor location.

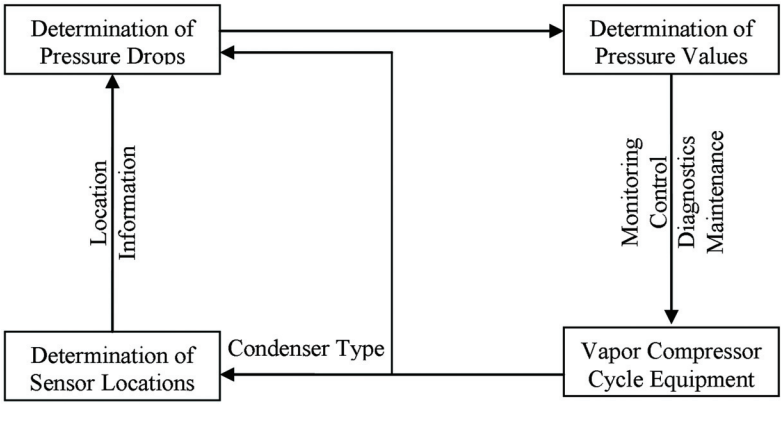

Figure 5. Overview of the virtual pressure sensors development concept.

where a saturated refrigerant temperature can be measured; the second step is to estimate the pressure drop between these locations and other locations where the pressure measurements are needed; finally, the virtual pressure values can be determined and used for monitoring, control, diagnostics, and maintenance of vapor-compression cycle equipment. Subsequent sections will follow this development strategy.

Identification of Temperature Sensor Locations

Condensers. The energy associated with desuperheating the refrigerant until it condenses accounts for about 10%–20% of the total condenser heat rejection. Since the desuperheating portion of the heat transfer has the largest temperature difference between the refrigerant and ambient, it typically only requires about three passes of the condenser to cool the refrigerant to the condensation point. Li and Braun (2007d) plotted the refrigerant temperature distribution in the condenser for all the testing data to visualize the refrigerant phase distribution in the condenser. Considering potential fault impacts, it was determined through extensive testing that it is safe to put the temperature sensor (*CT*) on a return bend that is one or two passes before the middle of the desuperheating/condensing circuit of a Type I condenser as depicted in Figure 2. This is typically at the fourth or fifth pass tube bend (Li and Braun 2007d). For a Type II condenser, it is typically safe to place the temperature sensor (*CT*) at the condensing manifold as shown in Figure 3.

Evaporators. Extensive testing was performed within the laboratory to track the location of two-phase sections within the evaporator for a range of operating conditions and levels of refrigerant charge. Li and Braun (2007d) plotted the refrigerant temperature distribution in the evaporator for all the testing data to visualize the refrigerant phase distribution in the evaporator. At normal refrigerant charge levels and in the absence of other faults, most of the evaporator (more than 70%) contains a two-phase mixture of refrigerant under steady-state conditions. However, when the refrigerant charge is low or the system is impacted by severe evaporator fouling, liquid line restriction, or compressor leakage, the refrigerant can be superheated after the first pass within the evaporator. Consequently, the only robust locations for the temperature measurement are at the entrance to the evaporator or on the first return bend after the first refrigerant pass through the HX. It is important to note that there can be a pressure drop at the entrance due to entrance effects so that the actual evaporating temperature can be a little lower than the refrigerant inlet temperature (Li and Braun 2007d). However, for this study it is recommended that a single temperature sensor (*ET*) be placed at the entrance of the evaporator as depicted in Figure 4.

Pressure Drop Estimation

Estimates of refrigerant pressure drops can be used to estimate virtual pressure measurements from saturation pressures determined using the surface-mounted refrigerant temperature measurements. Pressure drop in condensers and evaporators is due to two effects: friction and changes in fluid momentum with velocity changes. However, most of a pressure drop can be attributed to friction, which is approximately proportional to the square of the refrigerant mass flow rate, or

$$\Delta P = k\dot{m}_{ref}^2 , \tag{1}$$

where k is a proportionality constant.

For a unitary air conditioner or heat pump, the refrigerant mass flow rate primarily depends on the compressor discharge and suction pressures (P_{dis} and P_{suct}). However, compressor data is typically presented as a function of the refrigerant saturation temperatures associated with these

pressures, which can be termed the *discharge dew-point temperature* ($T_{dp,dis}$) and the *suction dew-point temperature* ($T_{dp,suct}$). The dew-point temperatures differ somewhat from the condensing and evaporating temperatures due to pressure drops.

For unitary air conditioners, $T_{dp,dis}$ ranges from about 80°F to 140°F (26.7°C to 60°C) and $T_{dp,suct}$ ranges from 20°F to 50°F (–6.7°C to 10°C). For unitary heat pumps, $T_{dp,dis}$ and $T_{dp,suct}$ range from about 80°F to 130°F (26.7°C to 54.4°C) and from about 10°F to 40°F (–12.2°C to 4.4°C), respectively. Typically, the system safety cutoff is triggered if these limits are reached. The refrigerant mass flow produced by the compressor increases with increasing suction dew-point temperature and decreasing discharge dew-point temperature. During most of the time, a system will operate at moderate suction and discharge dew-point temperatures: $T_{dp,suct}$ is about 35°F (1.7°C) and $T_{dp,dis}$ is about 115°F (46.1°C) for air conditioners, and $T_{dp,suct}$ is about 30°F (–1.1°C) and $T_{dp,dis}$ is about 100°F (37.8°C) for heat pumps. In this paper, these moderate dew-point temperatures are designated as the rated dew-point temperatures (see Table 1).

The refrigerant mass flow rate can be determined from a manufacturer's compressor map at the rated dew-point temperatures according to

$$\dot{m}_{ref,\,rated} = \text{compressor map}(T_{dp,\,dis,\,rated}, T_{dp,\,suct,\,rated}) \ . \tag{2}$$

Then, according to Equation 1, the pressure drop through a HX section can be evaluated in terms of actual and rated flow conditions according to

$$\Delta P = \Delta P_{rated}\left(\frac{\dot{m}_{ref}}{\dot{m}_{ref,\,rated}}\right)^2 , \tag{3}$$

where ΔP_{rated} is evaluated at $\dot{m}_{ref,\,rated}$.

In order to estimate the bounds on the pressure drop, it is useful to consider the range of refrigerant flows that may occur. Refrigerant flow rates deviate from the rated flow rate due to changes in refrigerant density at the compressor inlet and changes in volumetric efficiency with operating pressures. The range of flow rates can be expressed as

$$\alpha\dot{m}_{ref,\,rated} \le \dot{m}_{ref} \le \beta\dot{m}_{ref,\,rated} \ , \tag{4}$$

where the constants α and β depend on the type of compressor and the operating pressure range. Substituting Equation 4 into Equation 3 leads to an estimate of bounds for refrigerant pressure drop:

$$\alpha^2\Delta P_{rated} \le \Delta P \le \beta^2\Delta P_{rated} \tag{5}$$

Table 1. Compressor Suction and Discharge Dew-Point Temperatures

Compressor Operating Conditions		Air Conditioner	Heat Pump
Suction dew-point temperature, $T_{dp,suct}$, °F (°C)	Lower limit ($T_{dp,suct,ll}$)	20 (–6.7)	10 (–12.2)
	Upper limit ($T_{dp,suct,ul}$)	50 (10.0))	40 (4.4)
	Rated ($T_{dp,suct,rated}$)	35 (1.7)	30 (–1.1)
Discharge dew-point temperature, $T_{dp,dis}$, °F (°C)	Lower limit ($T_{dp,suct,ll}$)	80 (26.7)	80 (26.7)
	Upper limit ($T_{dp,suct,ul}$)	140 (60)	130 (54.4)
	Rated ($T_{dp,suct,rated}$)	115 (46.1)	100 (37.8)

Typical values of α and β for both air-conditioning and heat pump systems can be determined under the operating limits specified in Table 1 using compressor map data. For compressors with high volumetric efficiencies, such as a scroll compressor, α is approximately 0.7 and β is about 1.23. For low volumetric efficiency compressors, such as a reciprocating compressor, α and β are about 0.41 and 1.35, respectively. These parameters lead to the typical bounds for pressure drop (see Equations 6a and 6b). Although the typical values could vary slightly with different types of compressors, analyses presented in Figures 6–9 will be valid for any type of compressor whose performance falls in the bounds defined in Equation 6a or 6b.

$$0.5\Delta P_{rated} \le \Delta P \le 1.5\Delta P_{rated} \qquad \text{for high volumetric efficiency compressors} \tag{6a}$$

$$0.17\Delta P_{rated} \le \Delta P \le 1.83\Delta P_{rated} \qquad \text{for low volumetric efficiency compressors} \tag{6b}$$

A virtual pressure measurement is needed at the inlet to the compressor (i.e., compressor suction) in order to determine suction superheat for refrigerant charge evaluation and to characterize compressor performance. Since the evaporating temperature is measured near the inlet to the evaporator, it is necessary to have an estimate of the overall pressure drop on the low-pressure side of the system. For the low-pressure side of an air-conditioning system, the pressure drop through the evaporator and suction line at the rating condition, $\Delta P_{suct,rated}$, is relatively small and is typically in the range of 3 to 5 psi (20.7 to 34.5 kPa). For this range, Figure 6 illustrates the operating limits of the low-side pressure drop, ΔP_{suct}. For example, a system having $\Delta P_{suct,rated}$ = 4 psi (27.6 kPa) will have an operating range for ΔP_{suct} of about 2 to 6 psi (13.8 to 41.4 kPa) for a high volumetric efficiency compressor and a range from about 1 to 7 psi (6.9 to 48.3 kPa) for a low volumetric efficiency compressor. If $\Delta P_{suct,rated}$ were used to represent the actual ΔP_{suct}, then the maximum error is less than about 4 psi (27.6 kPa) for the worst case (systems with a low volumetric efficiency compressor operating under $\Delta P_{suct,rated}$ = 5 psi (34.5 kPa). For systems with a high efficiency compressor, the error will be less than about 2 psi (13.8 kPa) in many cases. Typically, actual pressure sensors used to measure P_{suct} for R-22 systems have a full scale of 400 psi (2758 kPa) and an accuracy of ±1% of full scale. This corresponds to a measurement error of ±4 psi (±27.6 kPa), which is comparable to the error caused by using $\Delta P_{suct,rated}$ to represent ΔP_{suct}.

Virtual pressure measurements are needed at two places on the high side of the system: 1) at the compressor discharge for use in characterizing compressor performance and 2) at the outlet of the condenser to determine subcooling for refrigerant charge evaluation. Since the surface temperature measurement is located near the middle of the coil, then it is necessary to estimate two pressure drops for the two virtual pressure measurements. The condenser and discharge line typically have a total pressure drop ranging from about 15 to 20 psi (103.4 to 137.9 kPa) at the rated condition. The pressure drop across the compressor discharge line and the desuperheating section of the condenser accounts for about half of the total pressure drop; the other half occurs within the two-phase and subcooled sections. Therefore, it is only necessary to estimate about half of the condenser pressure drop in determining virtual pressure measurements for compressor discharge and condenser outlet. Figure 7 illustrates the operating limits for the pressure drop from the compressor discharge to the location of the surface temperature measurement, ΔP_{dis}, and the pressure drop from the surface temperature measurement to outlet of the condenser, ΔP_{ll}. If rated values $\Delta P_{dis,rated}$ and $\Delta P_{ll,rated}$ were used to represent the actual pressure drops ΔP_{dis} and ΔP_{ll}, then the maximum error would normally be less than about 8 psi (55.2 kPa): 4 to 5 psi (27.6 to 34.5 kPa) and 6 to 8 psi (41.4 to 55.2 kPa) for high and low volumetric efficiency compressors, respectively. Typically, pressure sensors used to measure high-side pressures have a full scale of 500 psi (3447 kPa) for R-22 and 1000 psi (6895 kPa) for R-410a with an accuracy

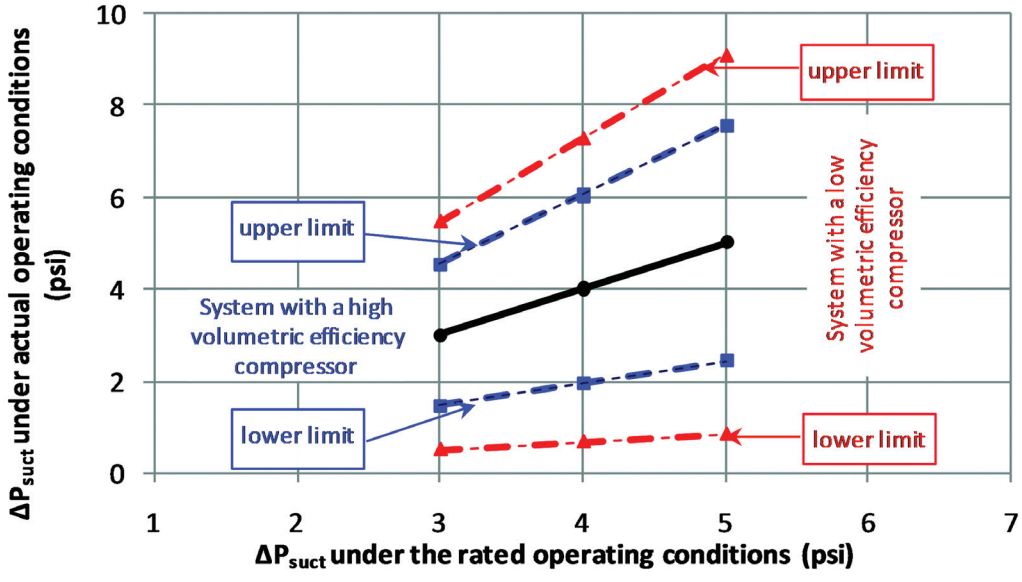

(a)

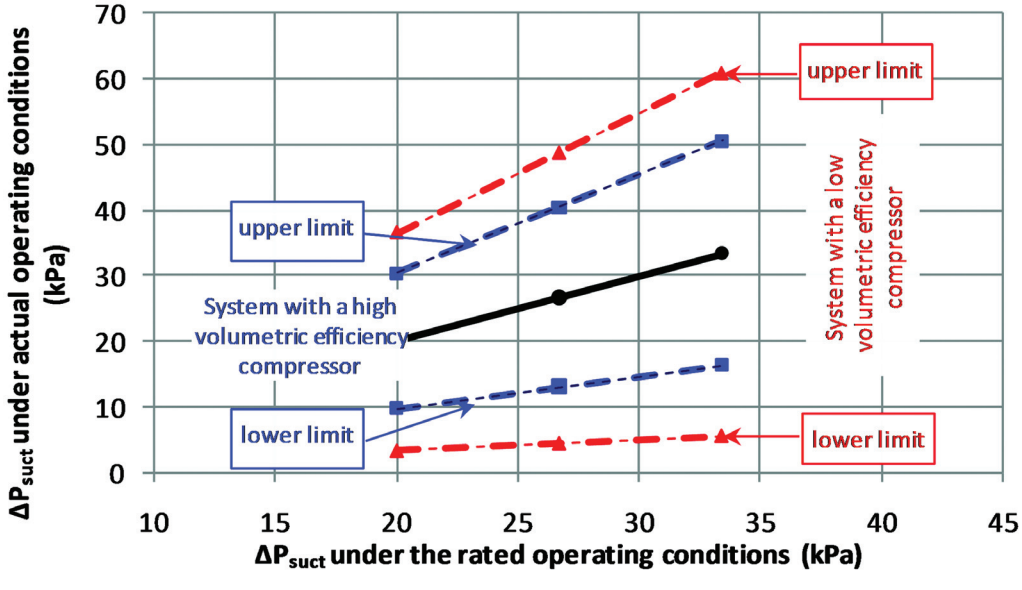

(b)

Figure 6. Approximate operating limits for low-side pressure drop, ΔP_{suct}, in unitary air conditioners: (a) I-P units and (b) SI units.

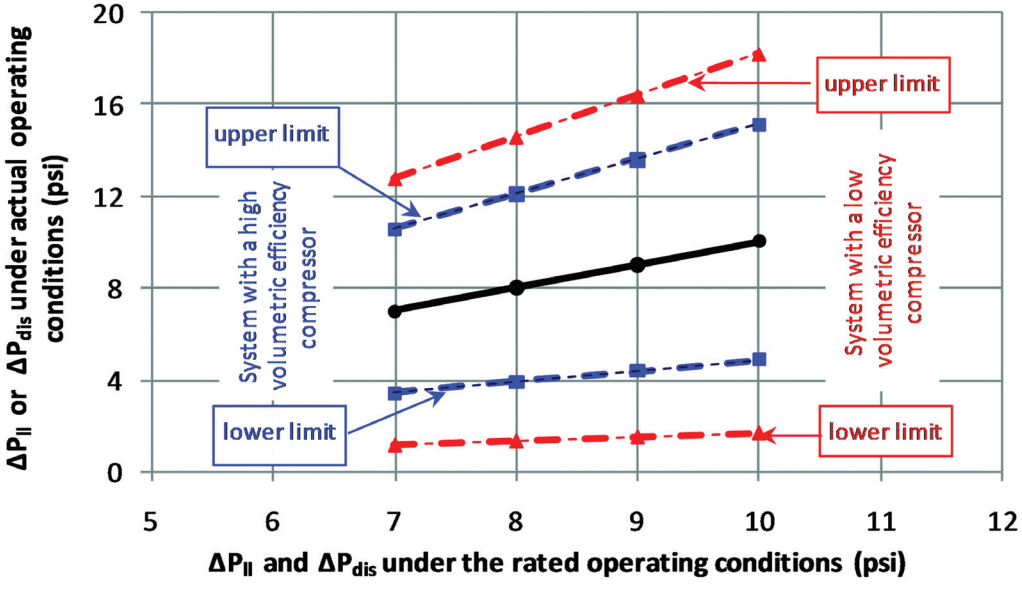

(a)

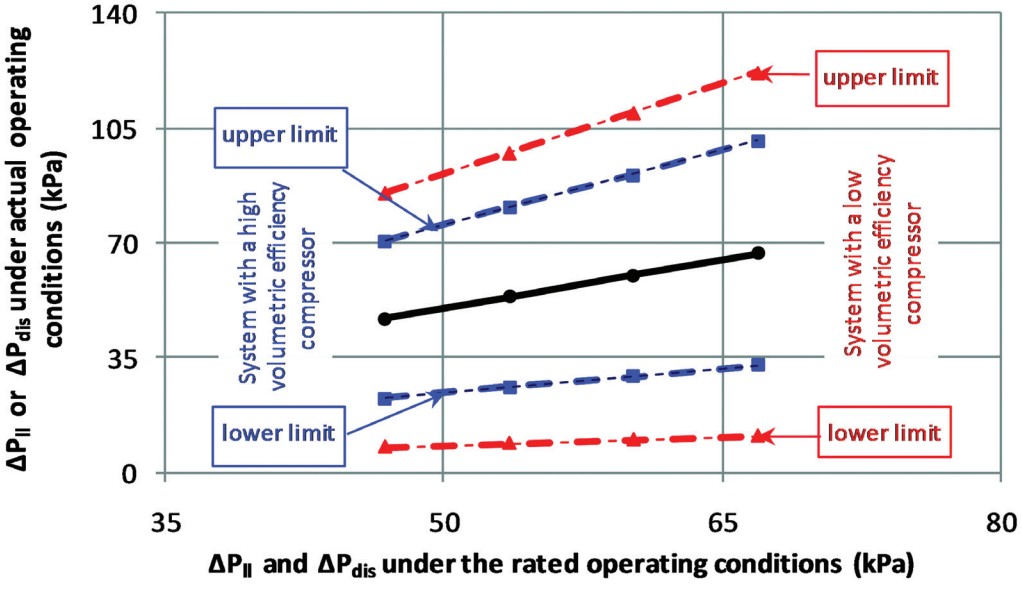

(b)

Figure 7. Approximate operating limits for pressure drop between compressor discharge and condensation section, ΔP_{dis}, and between condensing section and liquid line, ΔP_{ll}, for unitary air conditioners: (a) I-P units and (b) SI units.

of ±1% of full scale. Therefore, the measurement error associated with using a typical high-pressure sensor is from ±5 psi (±34.5 kPa) for R-22 to ±10 psi (±68.9 kPa) for R-410a, which is comparable to the error caused by using rating conditions to estimate high-side pressure drops.

Pressure drop within the evaporator of a heat pump operating in heating mode is generally larger than that for air conditioning because the evaporator is designed to operate as a condenser in cooling mode. Figure 8 illustrates the operating limits for low-side pressure within a heat pump operating in heating mode. The rated pressure drop, $\Delta P_{suct,rated}$, ranges from about 10 to 14 psi (68.9 to 96.5 kPa). If $\Delta P_{suct,rated}$ is used to represent the actual ΔP_{suct}, the maximum error ranges from about 5 to 8 psi (34.5 to 55.2 kPa) for systems with a high volumetric efficiency compressor and 8 to 12 psi (55.2 to 82.7 kPa) for systems with a low volumetric efficiency compressor. Consequently, the error caused by using $\Delta P_{suct,rated}$ to represent ΔP_{suct} is much higher than the measurement errors (±5 psi [±34.5 kPa] for R-22 and ±10 psi [±68.9 kPa] for R-410a) associated with an actual pressure sensor.

Conversely, when a heat pump operates in heating mode, the indoor unit serving as an evaporator in cooling mode is used as a condenser and the pressure drops are relatively small. Figure 9 illustrates the operating limits for the pressure drop between the discharge line and location of the surface temperature measurement, ΔP_{dis}, and the pressure drop between the surface temperature measurement and the liquid line, ΔP_{ll}. If $\Delta P_{dis,rated}$ and $\Delta P_{ll,rated}$ are used to represent the actual ΔP_{dis} and ΔP_{ll}, respectively, then the maximum error is generally less than 3 psi (20.7 kPa), which is small compared to the accuracy of directly measuring pressure (±5 psi [±34.5 kPa] or ±1% for a pressure sensor with a full scale of 0 to 500 psi [0 to 3447 kPa]).

In most situations, pressure drops at a representative rating condition can be used to determine virtual pressures regardless of the operating condition. However, for heat pumps operating in heating mode, Equation 3 could be used along with a compressor map to adjust the low-side pressure drop estimate, ΔP_{suct}, to account for variations in flow rate.

LABORATORY EVALUATIONS OF VIRTUAL PRESSURE SENSORS

System Descriptions

Laboratory data for three unitary air-conditioner systems and one heat pump system were used to evaluate the proposed virtual pressure sensor algorithms over a wide range of operating conditions. Surface-mounted temperature sensors were installed onto the tube bends of the HXs. Pressure sensors were installed to measure pressures at the suction to the compressor, discharge from the compressor, and liquid line leaving the condenser. Tables 2, 3, and 4 summarize the system information and range of testing conditions.

Virtual Sensor Accuracy

Virtual and actual pressure measurements were obtained for the range of conditions given in Tables 2–4 and the range of errors associated with the virtual pressure sensors, and other quantities determined from pressures were determined and are presented in Table 5 for the four different systems. In all cases, the error represents the difference between using the virtual pressure measurement and using an actual pressure measurement.

In general, virtual pressure sensors work very well for air-conditioning systems. Estimation errors are generally within ±1.6% for suction pressures and ±4.4% for compressor discharge and liquid line pressures. In addition, the errors associated with using virtual pressure measurements to determine subcooling, superheat, refrigerant mass flow rate, and compressor power consumption are relatively small for air-conditioning systems.

The accuracy of virtual pressure sensors for heat pumps in heating mode is not as good as that for air-conditioning systems, especially for suction pressure. The low-side pressure drop

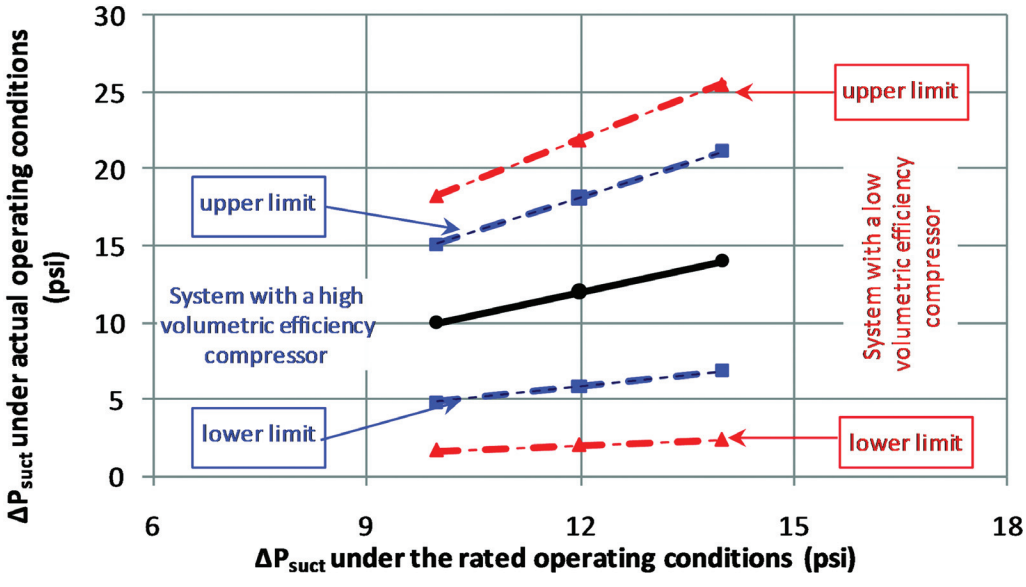

(a)

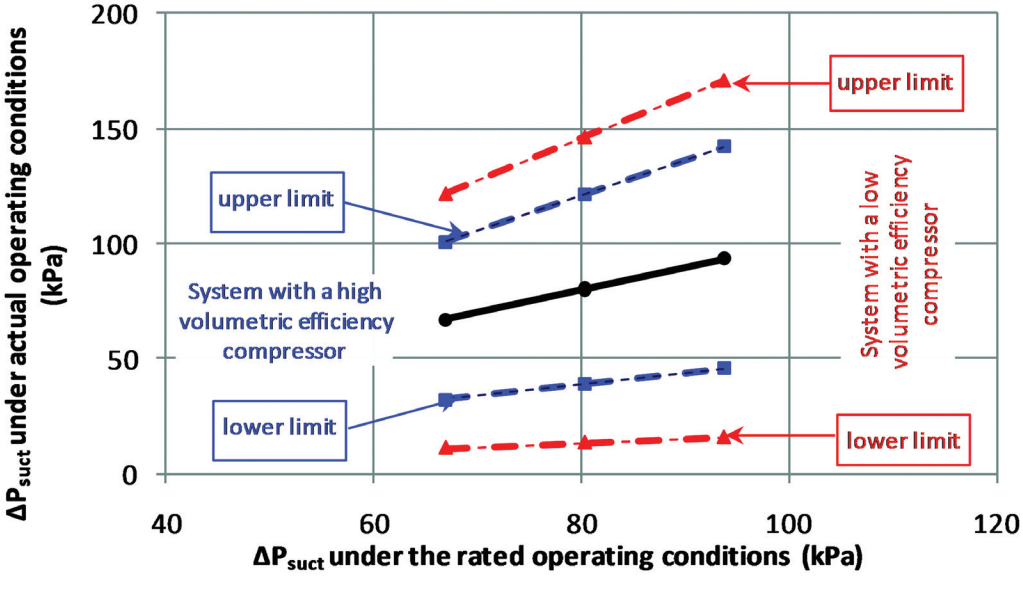

(b)

Figure 8. Approximate operating limits for low-side pressure drop, ΔP_{suct}, in unitary heat pumps operating in heating mode: (a) IP units and (b) SI units.

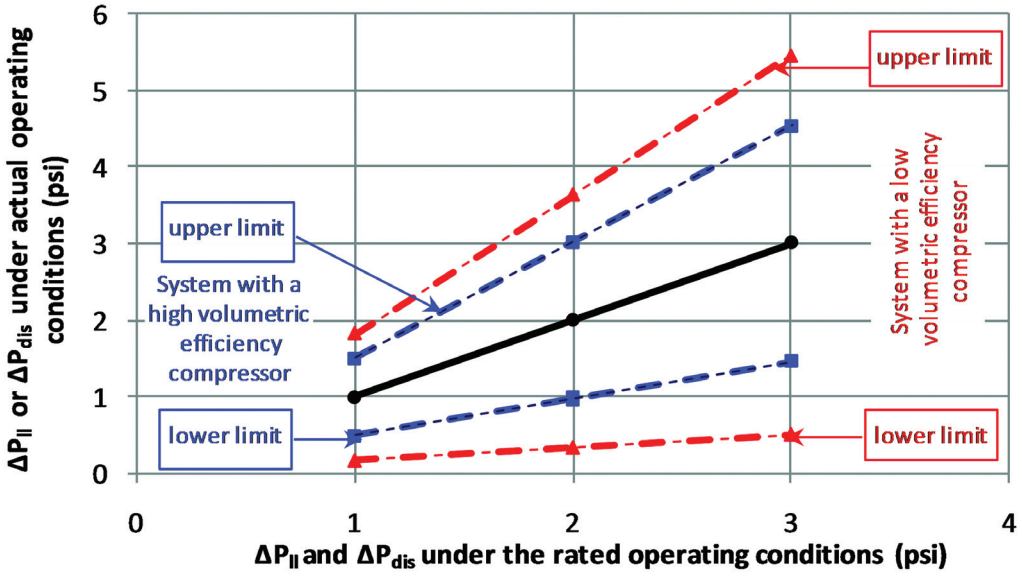

(a)

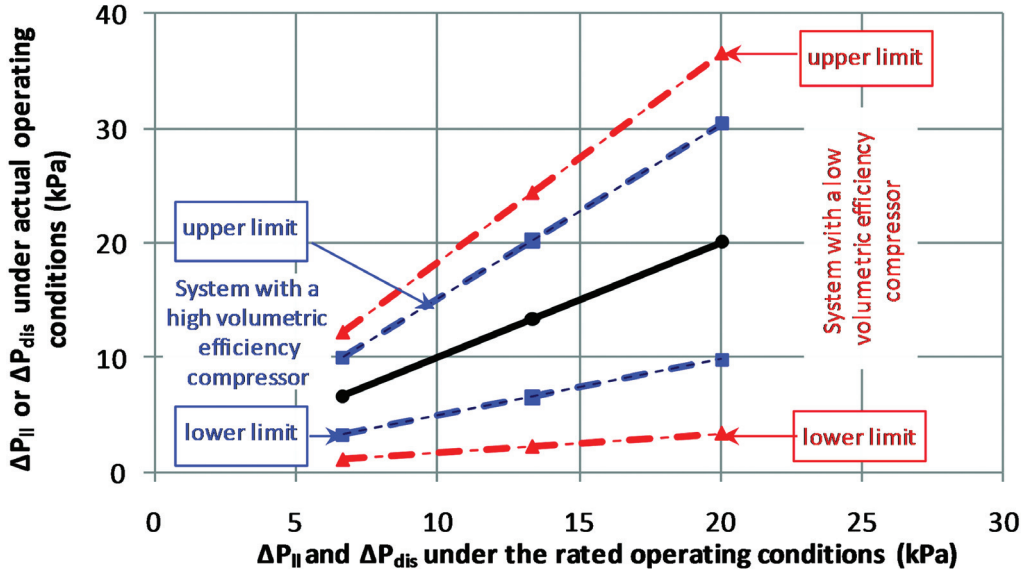

(b)

Figure 9. Approximate operating limits for pressure drop between compressor discharge and condensation section, ΔP_{dis}, and between condensing section and liquid line, ΔP_{ll}, in unitary heat pumps operating in heating mode: (a) IP units and (b) SI units.

Table 2. System Descriptions for Three Unitary Air Conditioners and One Heat Pump

System	Type	Size, ton (kW)	Refrigerant Type	Expansion Device	Assembling Type	Compressor Type
I	AC	3 (10.6)	R-410a	TXV	Split	Reciprocating
II	AC	3 (10.6)	R-410a	FXO	Split	Reciprocating
III	AC	3 (10.6)	R-410a	FXO	Packaged	Scroll
IV	HP	3 (10.6)	R-22	TXV	Split	Reciprocating

Note: TXV = thermostatic expansion valve, FXO = fixed orifice expansion device.

Table 3. Range of Testing Conditions for Three Unitary Air Conditioners

System	Charge Level, % of nominal	Outdoor Flow Rate, % of design	Indoor Flow Rate, % of design	Ambient Temperature, °F (°C)	Indoor Dry-Bulb Temperature, °F (°C)	Indoor Wet-Bulb Temperature, °F (°C)
I	57 to 113	35 to 100	50 to 100	80 to 125 (26.7 to 51.7)	80 (51.7)	60 to 75 (15.6 to 21.1)
II	58 to 130	100	45 to 130	80 to 125 (26.7 to 51.7)	80 (51.7)	54 to 73 (12.2 to 22.8)
III	61 to 141	32 to 100	50 to 140	80 to 125 (26.7 to 51.7)	80 (51.7)	54 to 73 (12.2 to 22.8)

Table 4. Range of Testing Conditions for Unitary Heat Pump in Heating Mode (System IV)

Charge Level, % of nominal	Outdoor Flow Rate, % of design	Indoor Flow Rate, % of design	Comp. Valve Leakage	Reversing Valve Leakage	Check Valve Leakage	Ambient Temp., °F (°C)	Indoor Dry-Bulb Temp., °F (°C)
70 to 130	60 to 100	65 to 135	0 to 20%	0 to 20%	0 to 20%	17 to 47 (–8.3 to 8.3)	70 (21.1)

Table 5. Range of Virtual Sensor Accuracies for Four Different Systems

Parameters	System I	System II	System III	System IV
Suction pressure	–0.8% to 1.5%	–1.5% to 0.3%	–0.8% to 1.6%	–3.6% to 8.9%
Discharge pressure	–2.3% to 2.1%	–2.4% to 3.4%	–1.6% to 0.4%	–4.8% to 3.6%
Liquid line pressure	–3.8% to 2.4%	–3.7% to 4.4%	–1.1% to 0.8%	–3.1% to 5.3%
Subcooling, °F (°C)	–2.8 to 1.9 (–1.6 to –1.1)	–2.3 to 3.4 (–1.3 to 1.9)	–0.8 to 0.6 (–0.4 to 0.3)	–2.2 to 3.9 (–1.2 to 2.2)
Superheat, °F (°C)	–0.9 to 0.4 (–0.5 to 0.2)	–0.2 to 0.8 (–0.1 to 0.4)	–0.9 to 0.5 (–0.5 to 0.3)	–5.3 to 2.0 (–2.9 to 1.1)
Compressor power consumption	–2.4% to 2.1%	–2.5% to 2.1%	–1.6% to 0.4%	–2.8% to 6.7%
Refrigerant flow rate	–0.9% to 2.2%	–3.0% to 1.2%	–1.1% to 2.1%	–6.7 to 14.4%

is considerably higher for heat pump heating than for air conditioning. Furthermore, it is more difficult to specify a reliable location for measuring condensing for heating mode because the refrigerant circuiting is optimized for cooling mode and each circuit is very short. However, the overall accuracy is reasonable in most cases.

Figure 10 shows comparisons between virtual and actual pressure measurements for data obtained with System I. Comparisons of other quantities determined using these virtual and actual pressure measurements are presented in Figures 11 and 12. In all cases, there is good agreement between virtual and actual pressure measurements and between the quantities derived

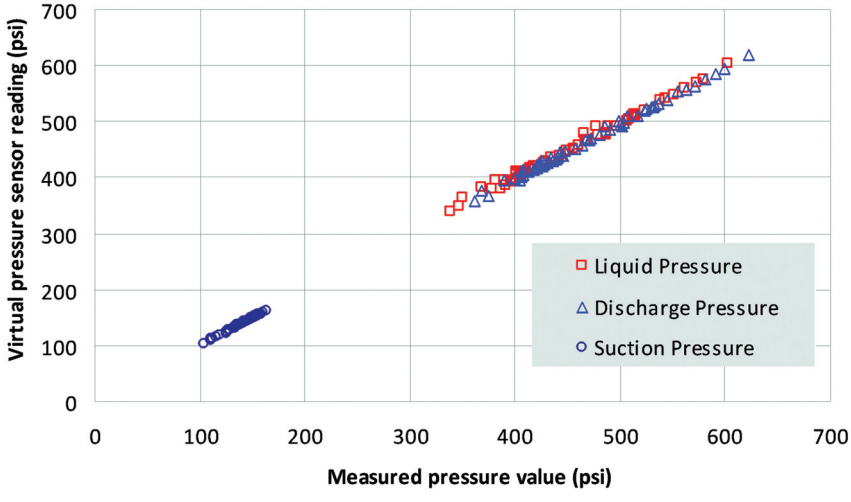

(a)

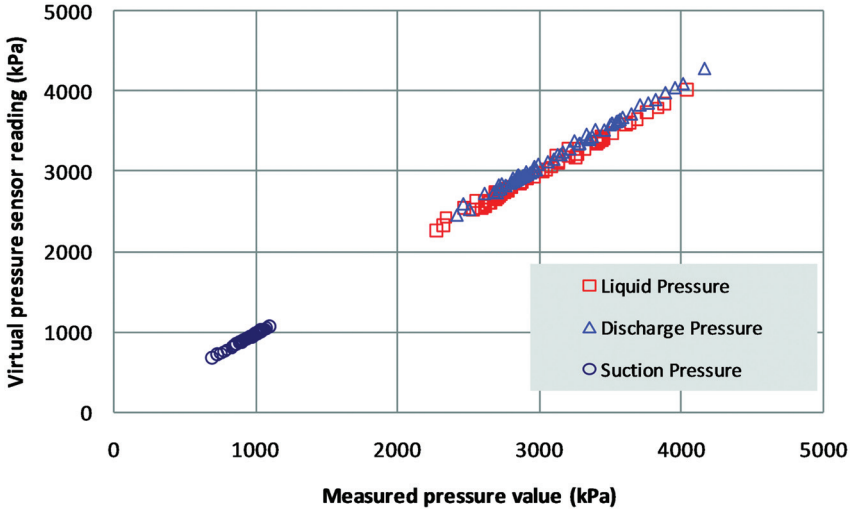

(b)

Figure 10. Comparisons of virtual and actual pressure measurements for System I: (a) IP units and (b) SI units.

from virtual and actual pressure measurements. In Figure 11, most of the results for superheat and subcooling are clustered in the range of 7°F to 14°F (–13.9°C to 10°C); however, there are some as high as 35°F (1.7°C), which correspond to faulty conditions such as low refrigerant charge. Unlike pressure and temperature, power consumption and refrigerant flow rate are non-property-extensive quantities and can be better presented in a normalized format. Unlike FDD features where normalization is based on fault-free conditions, indirect measurements of flow rate and power consumption are used to evaluate the impact by virtual pressure sensors and are normalized based on the maximum values of the data set.

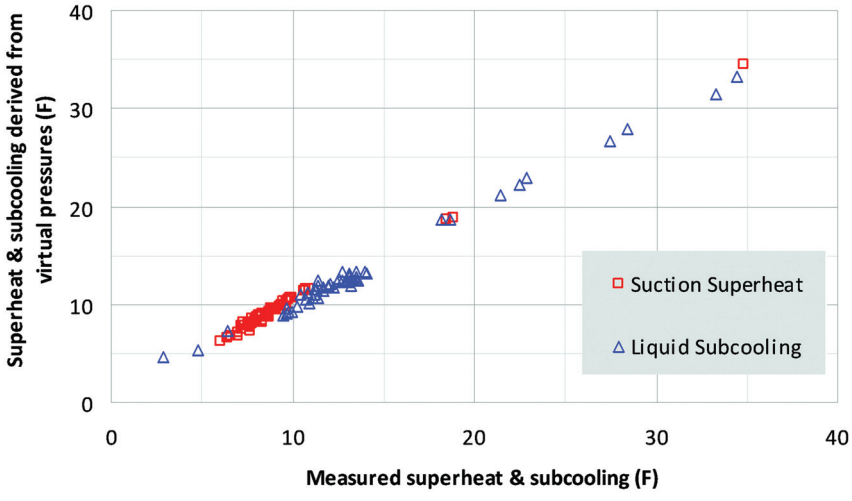

(a)

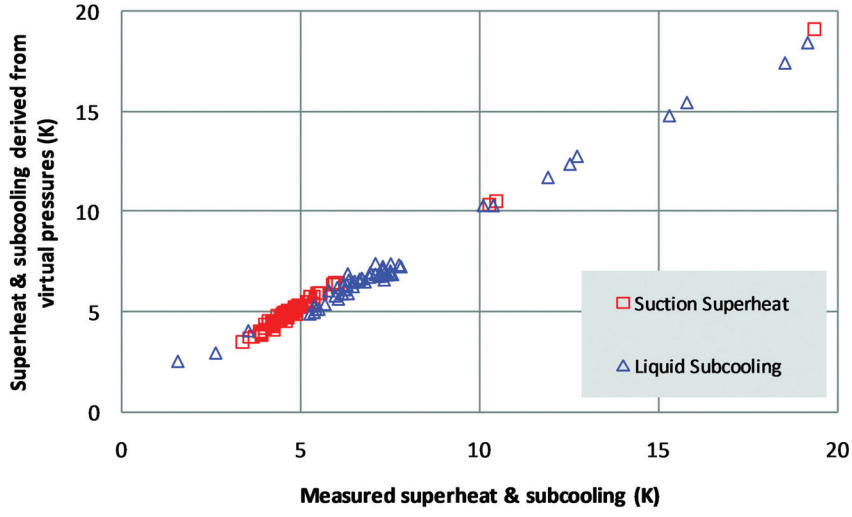

(b)

Figure 11. Suction superheat and liquid subcooling derived from actual and virtual pressure measurements for System I: (a) IP units and (b) SI units.

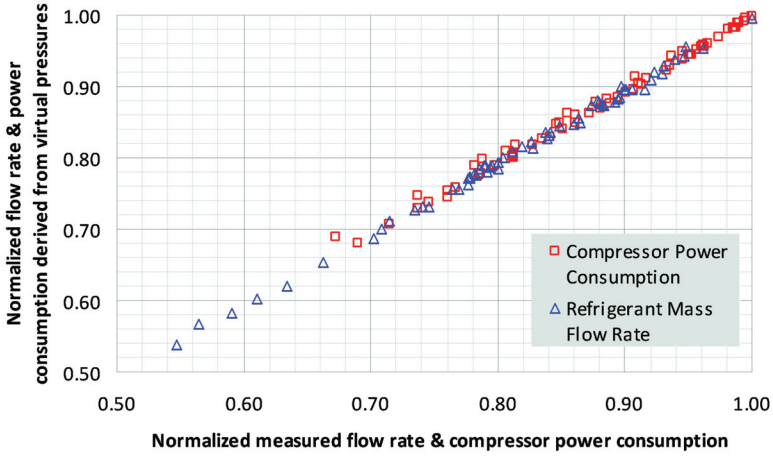

Figure 12. Compressor power consumption and refrigerant mass flow rate derived from actual and virtual pressure measurements for System I.

DIAGNOSING MULTIPLE SIMULTANEOUS FAULTS USING VIRTUAL PRESSURE SENSORS

Li and Braun (2007a) proposed a generic decoupling-based FDD method that can diagnose multiple simultaneous faults in vapor compression cycle equipment. Decoupling features are key to handling multiple simultaneous faults. Each decoupling feature is uniquely dependent on a certain individual fault and insensitive to impacts of other faults and changes in operating conditions. To this end, Li and Braun (2007b) developed decoupling features for those generic faults common in vapor compression cycle equipment, including outdoor HX fouling, improper indoor HX flow rate, compressor valve leakage, refrigerant under- or over-charge, noncondensable gases, and liquid line restriction faults (Breuker and Braun 1998). There are some faults unique to heat pumps, including reversing valve leakage and check valve leakage, whose decoupling features were recently developed by Li and Braun (2008).

The impact of virtual pressure sensors on FDD performance is evaluated through comparing outputs of the decoupling features determined with virtual pressure sensors to those determined with measured pressures. Figures 13–17 show the results. In these figures, compressor leakage refers to faults that degrade the volumetric efficiency of the compressor (e.g., leaky discharge valve), leading to reductions in refrigerant mass flow rate and cooling capacity. Fouling of the outdoor HX results from contaminants (e.g., dust) that are deposited on the coil surface, leading to reduced airflow and reduced exposed heat transfer surface area. Improper indoor HX flow rate could be caused either by improper test and balance during the commissioning process or, like outdoor HX fouling, by gradual deposition of air contaminants during the operating period. Refrigerant charge leakage refers to low refrigerant charge that impacts both cooling capacity and efficiency. In each figure, the rectangles centered at (0,0) represent thresholds for diagnosing faults. That is, a value of the diagnostic feature within ±0.2 corresponds to a no-fault condition for the particular fault associated with that figure; a value of indicators less than –0.2 means leakage for the compressor, low charge for refrigerant charge levels, fouling for outdoor HX, and low flow rates for indoor HX; a value of indicators larger than +0.2 means heat loss for a compressor, high charge for refrigerant charge levels, and excessive airflow rate for indoor and

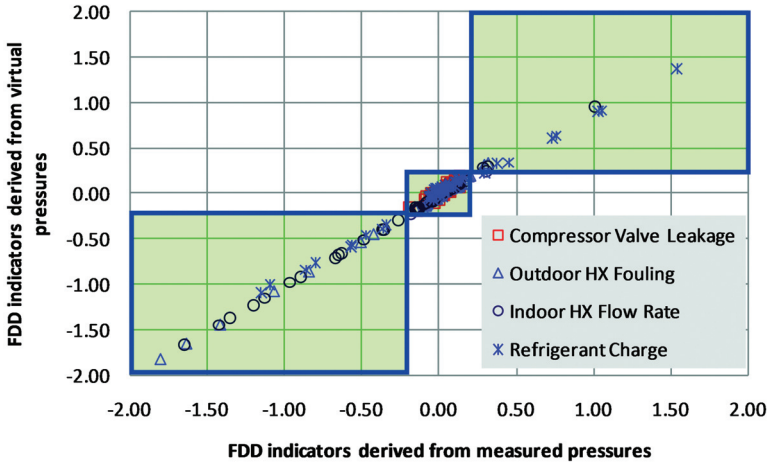

Figure 13. Comparison of FDD indicators derived from actual and virtual pressure measurements for System I.

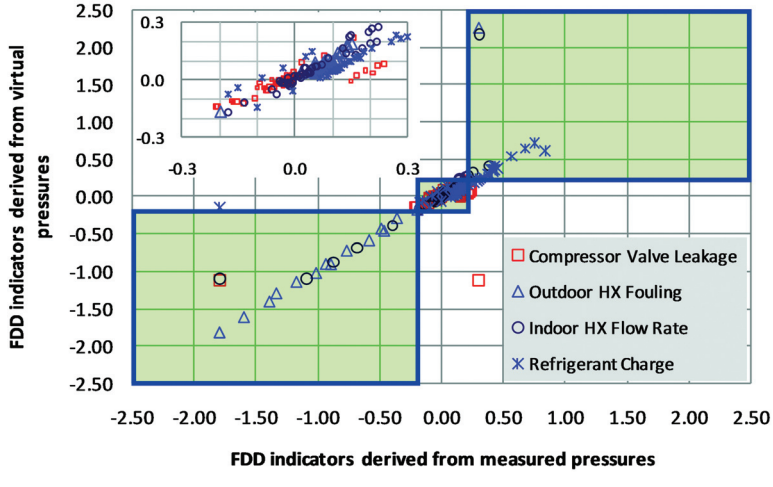

Figure 14. Comparison of FDD indicators derived from actual and virtual pressure measurements for System II.

outdoor HXs. For each case, individual fault levels were varied over a range of operating conditions, and combinations of indoor HX fouling and abnormal charge faults were considered.

Figure 13 compares the diagnostic fault indicators derived from measured pressures to those determined from virtual pressures for System I. For this system, there would be no loss in diagnostic sensitivity and no false alarms introduced by employing the virtual pressure sensors.

Figure 14 shows similar results for System II. However, the negative impact of using virtual sensors is a bit greater. There are three outliers where the indicator values determined using virtual pressure sensors do not match those determined from actual pressure measurements. One would generate false alarm for compressor leakage. One would cause a false alarm for an abnormally high indoor HX flow rate. One would indicate an abnormally high outdoor HX

flow rate, which is an impossible and undefined operating condition and thus can be artificially filtered to avoid false alarms. In addition, there are several points where the indicator values determined using virtual pressure sensors are slightly different than those determined from actual pressure measurements, two of which would result in a lack of diagnosis of compressor valve leakage when this fault is present and three of which would cause false alarms for high indoor HX flow rates. These slight mismatches are caused by the uncertainties in the virtual pressure sensors. Fortunately, the resulting false alarm would not lead to severe consequences because the indicated fault severity level is very low and no actions would be recommended; the resulting lack of diagnosis would not incur significant penalty because the actual fault severity level is low and its economic impact is surpassed by the savings for replacing real pressure sensors with virtual ones.

Figure 15 shows diagnostic indicator comparisons for System III. Overall, the agreement between indicators determined from virtual and actual pressure measurements is very good (the R-squared value of the first-order linear regression is 0.9938). There is some scatter in the data for the compressor leakage fault given in Figure 15. However, there would be no false alarms for these data points. Also, there would be no sensitivity loss or false alarms caused by virtual pressure sensors for the other three faults.

Heat pumps have all the same faults that occur for air conditioners with additional faults associated with components that accommodate the heating mode, including reversing valve leakage and check valve leakage. Figure 16 compares indoor HX flow rate, outdoor HX fouling, refrigerant charge, and compressor valve leakage fault indicators derived from measured pressures to those determined from virtual pressures for the heat pump system operating in heating mode (System IV). There would be neither sensitivity loss nor false alarms when using virtual pressure sensors to diagnose compressor valve leakage. Approximately six of the 75 points would result in missed diagnoses for indoor HX fouling or low flow rate setting (i.e., points falling outside the thresholds when using actual pressures but within the thresholds when using virtual pressures), and one of the 75 points would result in a false alarm (i.e., points falling inside the thresholds when using actual pressures but outside the thresholds when using virtual pressures). There is also some scatter in the comparisons between indicators for outdoor HX fouling. However, there would be no incorrect

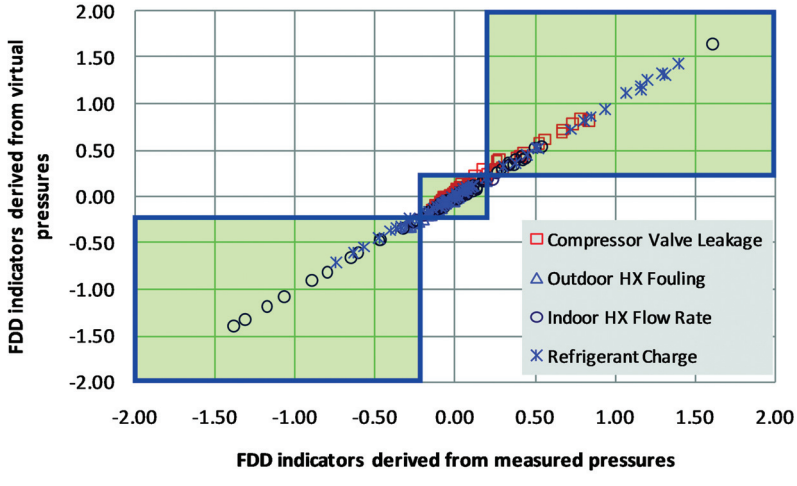

Figure 15. Comparison of FDD indicators derived from actual and virtual pressure measurements for System III.

diagnoses. Diagnostic performance for refrigerant charge would be very robust using virtual pressure sensors.

Figure 17 compares the fault indicators for check and reversing valve leakage derived from measured pressures to those determined from virtual pressures. There is neither sensitivity loss nor false alarms on check valve leakage or reversing valve leakage caused by virtual pressure sensors. This is because the feature for diagnosing check valve leakage in a thermostatic expansion valve heat pump system is a simple and unique function of superheat, which is affected only by the virtual suction pressure sensor. That is, errors in the other four virtual pressure sensors do not affect the diagnosis of check valve leakage. The diagnosis of reversing valve leakage uses pressures only indirectly for estimating refrigerant mass flow rate.

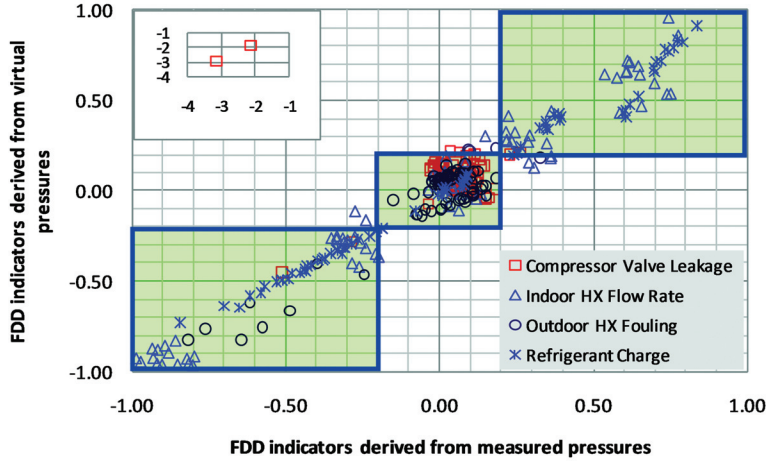

Figure 16. Comparison of FDD indicators derived from actual and virtual pressure measurements for a heat pump system.

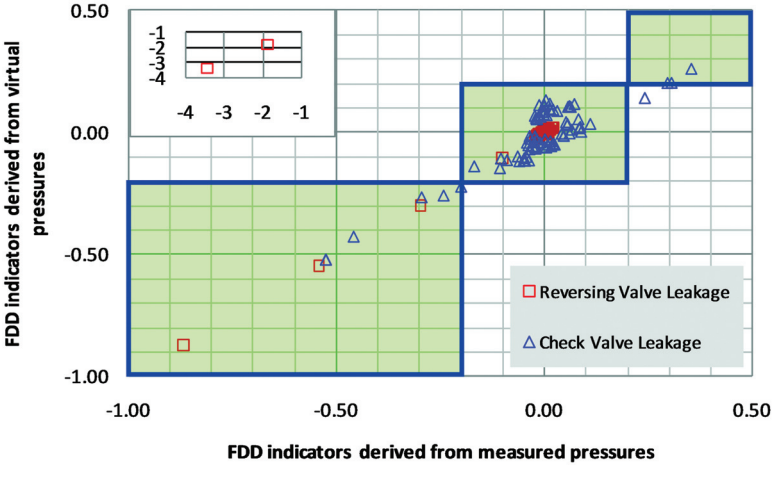

Figure 17. Comparison of FDD indicators derived from actual and virtual pressure measurements for a heat pump system.

CONCLUSION

Refrigerant pressures are important for monitoring, control, optimization, and diagnostics of vapor compression cycle equipment. However, the use of permanently mounted pressure sensors is expensive due to both sensor hardware and installation and can lead to refrigerant leakage when applied for retrofits. This paper described methods for inferring pressures from low-cost surface-mounted temperature measurements. The key issues that were addressed in the development included identification of appropriate locations for measuring saturation refrigerant temperatures and correcting for pressure drops to allow pressure estimates at other locations of interest. Experimental evaluation demonstrated that the virtual pressures have comparable accuracy to direct pressure measurements and work well when used for fault detection and diagnoses.

REFERENCES

Breuker, M.S., and J.E. Braun. 1998. Common faults and their impacts for rooftop air conditioners. *HVAC&R Research* 4(3):303–18.

Cui, J.T., and S.W. Wang. 2005. A model-based online fault detection and diagnosis strategy for centrifugal chiller systems. *International Journal of Thermal Sciences* 44(10):986–99.

Li, H., and J.E. Braun. 2003. An improved method for fault detection and diagnosis applied to packaged air conditioners. *ASHRAE Transactions* 109(2):683–92.

Li, H., and J.E. Braun. 2006. Evaluation of a decoupling-based fault detection and diagnostic technique—Part II: Field evaluation and application. *Journal of Harbin Institute of Technology* 13(Suppl):164–71.

Li, H., and J.E. Braun. 2007a. A methodology for diagnosing multiple-simultaneous faults in vapor compression air conditioners. *HVAC&R Research* 13(2):369–95.

Li, H., and J.E. Braun. 2007b. Decoupling features and virtual sensors for diagnosis of faults in vapor compression air conditioners. *International Journal of Refrigeration* 30(3):546–64.

Li, H., and J.E. Braun. 2007c. An economic evaluation of the benefits associated with application of automated fault detection and diagnosis in rooftop air conditioners. *ASHRAE Transactions* 113(2):200–10.

Li, H., and J.E. Braun. 2007d. Development, implementation, and deployment of automated fault detection and diagnostics for vapor compression equipment. Final Report, no. 03-STAC-01, State Technologies Advancement Collaborative (STAC).

Li, H., and J.E. Braun. 2008. Decoupling features for diagnosis of reversing and check vales faults in heat pumps. *International Journal of Refrigeration* 32(2):316–26.

Reddy, T.A. 2007. Application of a generic evaluation methodology to assess four different chiller FDD methods. *HVAC&R Research* 13(5):711–29.

Rossi, T.M., and J.E. Braun. 1997. A statistical, rule-based fault detection and diagnostic method for vapor compression air conditioners. *HVAC&R Research* 3(1):19–37.